Supplementary Information

Structures of Th^{4+} Aqueous Solutions: Insights from AIMD and Metadynamics Simulations

Yang He[a], Jun-Bo Lu[b,c], Yang-Yang Zhang[b], Han-Shi Hu[*a], Jun Li[*a,b,c]

[a]Department of Chemistry and Engineering Research Center of Advanced Rare-Earth Materials of Ministry of Education, Tsinghua University, Beijing 100084, China.

[b]Department of Chemistry and Guangdong Provincial Key Laboratory of Catalytic Chemistry, Southern University of Science and Technology, Shenzhen 518055, China

[c]Fundamental Science Center of Rare Earths, Ganjiang Innovation Academy, Chinese Academy of Sciences, Ganzhou 341000, China.

Corresponding Author:

*E-mail: hshu@mail.tsinghua.edu.cn

*E-mail: junli@mail.tsinghua.edu.cn

Computation Details:

AIMD simulations.

To investigate the effects of temperature and Th^{4+} ions on the structure of the solution, we have conducted simulations with three-dimensional periodic boundary conditions in a 12.42 * 12.42 * 12.42 Å simulation box. The initial settings of these simulations were as follows:

1. 64 water molecules (pure water), at 298.15K
2. $Th(H_2O)_9^{4+}$ and 55 water molecules, at 298.15K
3. $Th(H_2O)_9^{4+}$ and 55 water molecules, at 323.15K
4. $Th(H_2O)_9^{4+}$ and 55 water molecules, at 363.15K
5. $Th(H_2O)_9^{4+}$, 55 water molecules and 4 evenly placed Cl^-, at 298.15K
6. $Th(H_2O)_9^{4+}$, 55 water molecules and 4 evenly placed Br^-, at 298.15K
7. $Th(H_2O)_9^{4+}$, 55 water molecules and 4 evenly placed NO_3^-, at 298.15K
8. $Th(H_2O)_9^{4+}$, 55 water molecules and 4 evenly placed ClO_4^-, at 298.15K
9. $Th(H_2O)_{10}^{4+}$ and 54 water molecules, at 298.15K

Simulation no. 9 was conducted with equilibrium phase simulation for 5 ps and the change from 10-coordination to 9-coordination happened rapidly, so the subsequent production phase simulation was not conducted. The time information of simulations is shown in Table S1.

Table S1. Time Information of Simulations

simulation(s)	equilibrium phase	production phase
1	over 5 ps	15 ps
2-4	2 ps	20 ps
5, 8	5 ps	20 ps
6, 7	over 3 ps	20 ps
9	5 ps	—

Metadynamics method.

Metadynamics is a computational technique used to enhance the sampling of rare events in molecular dynamics simulations. This method is particularly effective in exploring complex free energy surface (FES), overcoming the limitations of conventional molecular dynamics by accelerating the occurrence of rare events. It is achieved by periodically adding an external history-dependent bias Gaussian potential to the Hamiltonian of the system, based on the values of selected collective variables (CVs) that describe the state of the system. The added Gaussian potentials prevent the system from revisiting the sampled configurations, thereby pushing it to explore new regions of the CVs space. The FES can be reconstructed from these bias potentials, providing insights into the thermodynamics and kinetics of the system. Metadynamics has been widely used in the previous studies, offering a powerful tool for understanding and predicting the behavior of complex systems. Its application in our study aids in elucidating the stability and dynamics of the hydrated Th^{4+} ion in different coordination environments in the aqueous solution.

The CVs are defined as a set of N functions of the system coordinates *R*:

$$S(R) = (S_1(R), \dots, S_N(R))$$

which are utilized to characterize the state of the system. Ideal CVs should be capable of distinguishing between reactant, transition, and product states in the reaction, and should be able to describe the kinetics of the reaction. The common CVs include interatomic distances, bond angles, dihedral angles, and intermolecular distances. Assuming a CV, $s(R)$, has been selected, the value of metadynamics bias potential at time t, $V(s, t)$, is given by:

$$V(s,t) = \sum_{t'<t} W exp(-\frac{(s(R) - s(R(t'))}{2\sigma^2})$$

where W and σ are respectively the height and width of the Gaussian for $s(R)$, times $t' = \tau, 2\tau, \dots, M\tau$, and τ is the time interval for adding the Gaussian bias potentials. When the time t is sufficiently large, the bias potentials provide an unbiased estimate of the free energy along $s(R)$:

$$F(s) = -\lim_{t\to\infty} V(s,t) + Constant$$

1. One-dimensional free energy (1D FES) surface using $CN_{Th\text{-}O}$ as the CV

In this work, we initially utilize the primary Th-O coordination number ($CN_{Th\text{-}O}$) as the CV to investigate the possible hydration numbers of Th^{4+} in the aqueous solution. The functional form of $CN_{Th\text{-}O}$ is as follows:

$$CN_{Th-O} = \sum_{i=1}^{n_O} \frac{1-\left(\frac{R_{Th-O}}{R_0}\right)^n}{1-\left(\frac{R_{Th-O}}{R_0}\right)^m} = \sum_{i=1}^{n_O} s_i(R_{Th-O})$$

where n_O is the number of oxygen atoms in the system, $R_{Th\text{-}O}$ is the Th-O distance, R_0 = 3.4 Å, n = 23, m = 46. These parameters are set such that the function $s_i(R_{Th\text{-}O})$ smoothly decays from one to zero in the region between the first and second solvation shells (see Fig, S1). Based on the well-equilibrated trajectories, the metadynamics simulations were performed with the following parameters: W = 0.5 kcal/mol, σ = 0.05, τ = 20 fs (40Δt).

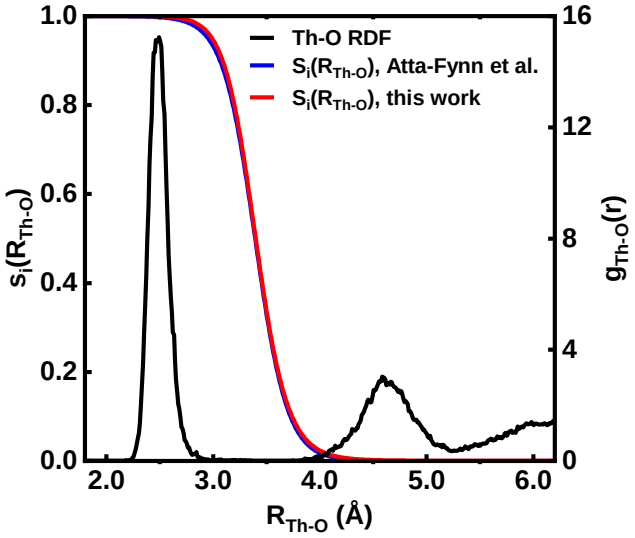

Fig. S1. Depiction of $s_i(R_{Th\text{-}O})$ used in the current work. Th-O RDF obtained from the simulation of the system with $Th(H_2O)_9^{4+}$ are shown for comparison.

Three metadynamics simulations, each with a duration of 100 ps, were conducted with different initial configurations. Initially, the convergence of a single metadynamics simulation must be assessed. It is already known that if the sampling time is sufficiently large, the sum of all bias Gaussian potentials can serve as an unbiased estimate of the FES. The main challenge is that it is difficult to determine at which moment this sum

will accurately reconstruct the FES. In fact, it is generally believed that when a metadynamics simulation has converged, the reconstructed FES (or history-dependent bias potentials) obtained at different sampling times should be similar, as noted in previous studies.[1-3] A simple approach is to look for convergence trends based on changes in the reconstructed FES with respect to sampling time. In this work, we calculated and compared the FES reconstructed at sampling times of 20, 40, 60, 80, and 100 ps. To quantify the similarity of the results at different sampling times, the results are divided into three intervals: 20 ~ 60 ps, 40 ~ 80 ps, and 60 ~ 100 ps, calculating the standard deviations (A_{error}) for each. As shown in Fig. S2, the values of A_{error} across most regions of the FES are less than 5 kcal/mol for the 60 ~ 100 ps interval, indicating good convergence of the metadynamics in this time interval.

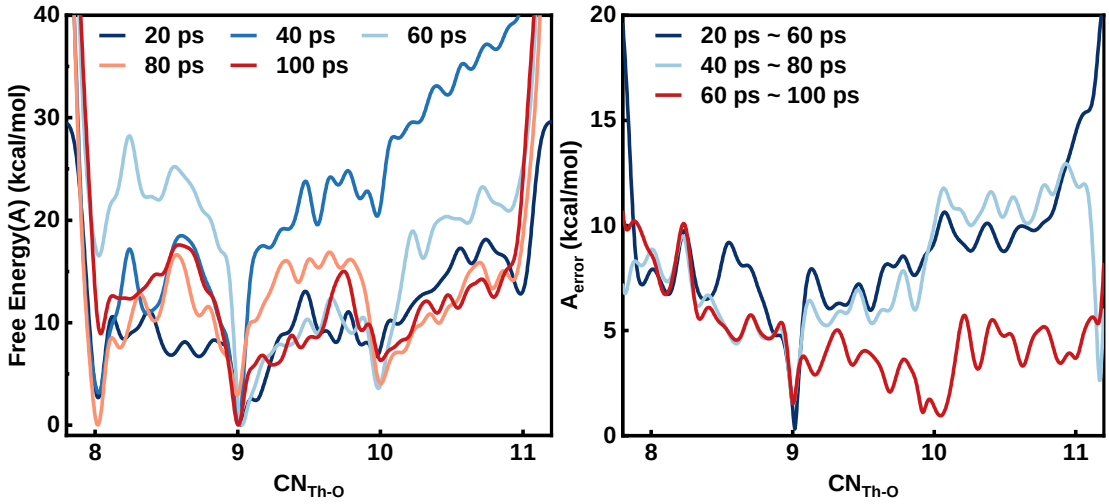

Fig. S2. Temporal convergence of 1D FES obtained from the metadynamics simulation.

To mitigate the randomness in a single simulation, the final values of free energy were obtained using the average of results from these three independent metadynamics simulations, with the standard deviation provided for each point (see Fig. 2). The mean standard deviation is 4.62 kcal/mol, indicating a relatively good convergence of these statistical average results. Moreover, a comparison is made between the average (A*) of the converged single simulation within the 60 ~ 100 ps sampling interval (in red) and the statistical average (A) of the three independent simulations reported in the current work (in black), which shows a close agreement (see Fig. S3).

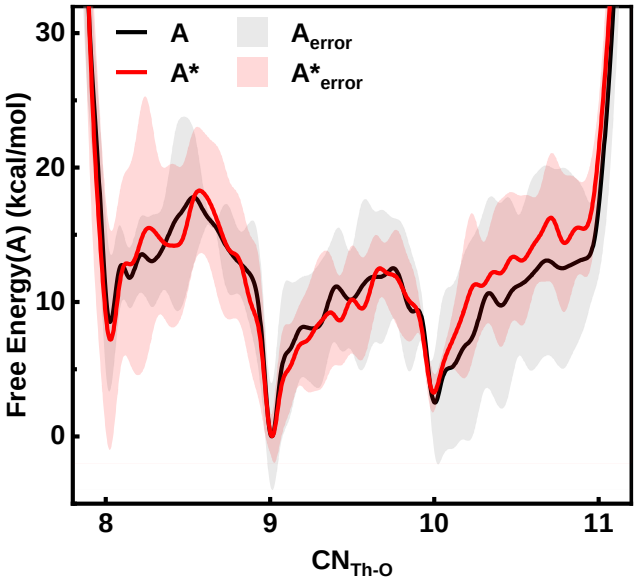

Fig. S3. FES results from the single converged metadynamics simulation (in red) and the statistical average of the three independent metadynamics simulations (in black).

2. Two-dimensional free energy surface (2D FES) using $r_{Th\text{-}Cl}$ and $CN_{Th\text{-}O}$ as CVs.

To investigate whether counterions directly coordinate with the Th^{4+} ion in the aqueous solution, we select the Th^{4+} - $4Cl^-$ - $64H_2O$ system for investigation. Metadynamics simulations, using the Th-Cl distance ($r_{Th\text{-}Cl}$) and $CN_{Th\text{-}O}$ as CVs, are applied to reconstruct the two-dimensional FES associated with different forms of Th^{4+} - Cl^- ion pairs in the aqueous solution. Appropriate constraints are used to to the CVs in the simulations to ensure that the resulting two-dimensional FES corresponds only to the simplest scenario of a single Cl^- ion replacing a single water molecule. Specifically, based on different values of the two CVs $r_{Th\text{-}Cl}$ and $CN_{Th\text{-}O}$, several forms of potential ion pairs (marked with letter labels in the Fig. 6) can be identified in the 2D FES:

$$Cl^- \overset{r_{Th\text{-}Cl}}{\longleftrightarrow} Th(H_2O)^{4+}_{CN_{Th\text{-}O}} + 3Cl^-$$

	$r_{Th\text{-}Cl}$ (Å)	$CN_{Th\text{-}O}$	state
A	4.0 ~ 6.0	9	$Th(H_2O)_9^{4+} + 4Cl^-$ **(SIPs)**
B	4.0 ~ 6.0	8	$Th(H_2O)_8^{4+} + 4Cl^- + H_2O$
C	2.5 ~ 3.0	9	$Th(H_2O)_9Cl^{3+} + 3Cl^-$
D	2.5 ~ 3.0	8	$Th(H_2O)_8Cl^{3+} + 3Cl^- + H_2O$ **(CIPs)**

Two thermodynamically stable states (states A and D in the Fig. 6) identified in the 2D FES are further illustrated in the Fig. S4. During the sampling process, the transition begins from the SIPs state (state A) where Th^{4+} and Cl^- are not in direct contact. A single Cl^- ion approaches Th^{4+}, leading to the occurrence of ligand substitution and formation of the CIPs state (state D) where Th^{4+} and Cl^- are directly bonded.

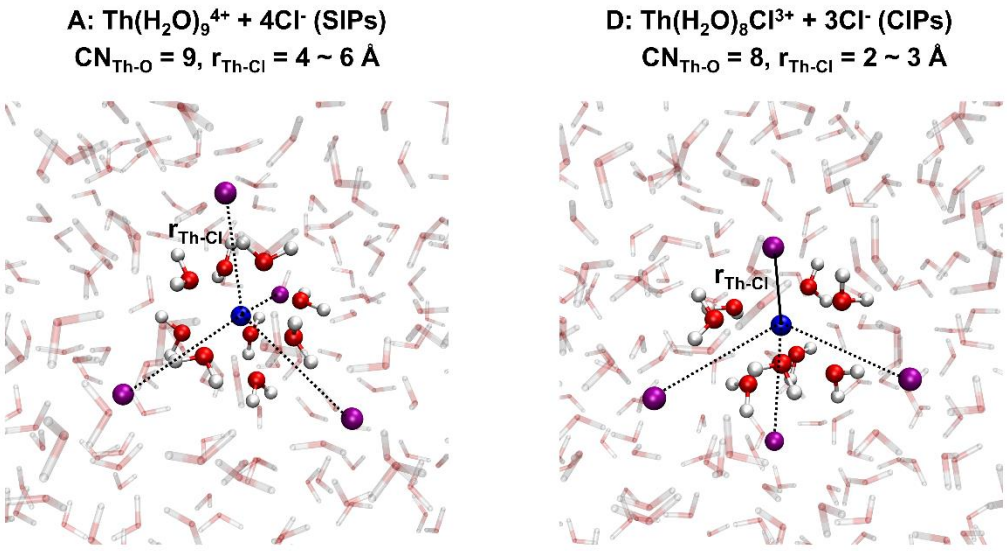

Fig. S4. SIPs (left) and CIPs (right) states identified in the 2D FES. The figure highlights the Th^{4+} ion (in blue) and the water molecules in the FSS (oxygen atoms in red, hydrogen atoms in white). Cl^- ions in the SSS are also shown (in purple). During the metadynamics simulation, bias potentials are added to one Cl^- ion to facilitate its closer approach to Th^{4+}, forming the CIPs state. The distance between this Cl^- ion and Th^{4+} corresponds to $r_{Th\text{-}Cl}$ in the CVs, while the number of first-shell water molecules corresponds to $CN_{Th\text{-}O}$ in the CVs.

In the metadynamics calculations, the following common parameters were used for both CVs: W = 0.5 kcal/mol, σ = 0.1, τ = 20 fs (40Δt). Similarly, three metadynamics simulations, each with a duration of 180 ps, were conducted with different initial configurations. The final values of free energy were obtained using the average of these three sets of data, with the standard deviation provided for each point (see Fig. S5). The convergence of a single simulation (with sampling times of 140, 160, and 180 ps) was also assessed (see Fig. S6). The 2D FES obtained within the time range of 140 ~ 180

ps exhibits standard deviations of less than 5 kcal/mol in the majority of regions, indicating that the metadynamics simulation achieved good convergence during this time interval. Finally, the results of the converged single simulation were compared with the statistical average results from three independent simulations, showing a good agreement (see Fig. S7).

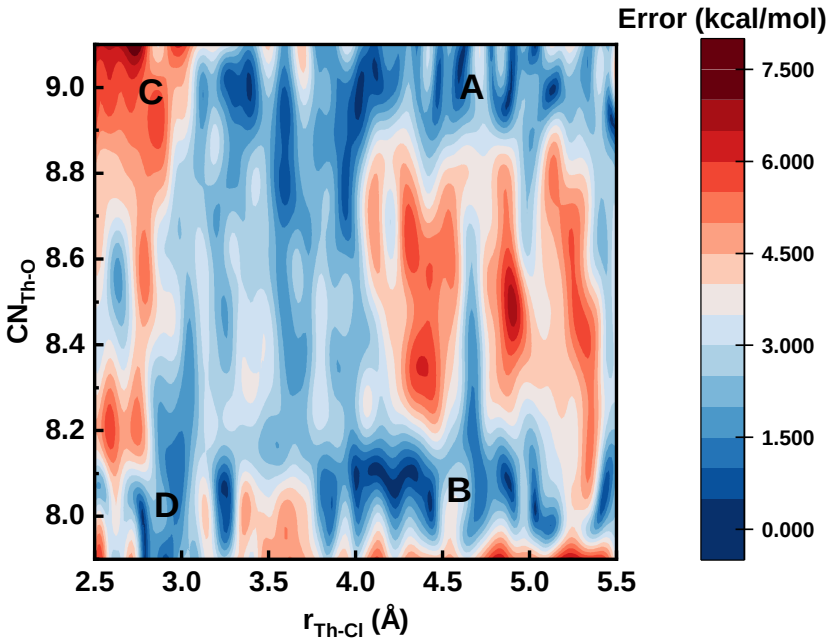

Fig. S5. Standard deviation for each point in the 2D FES.

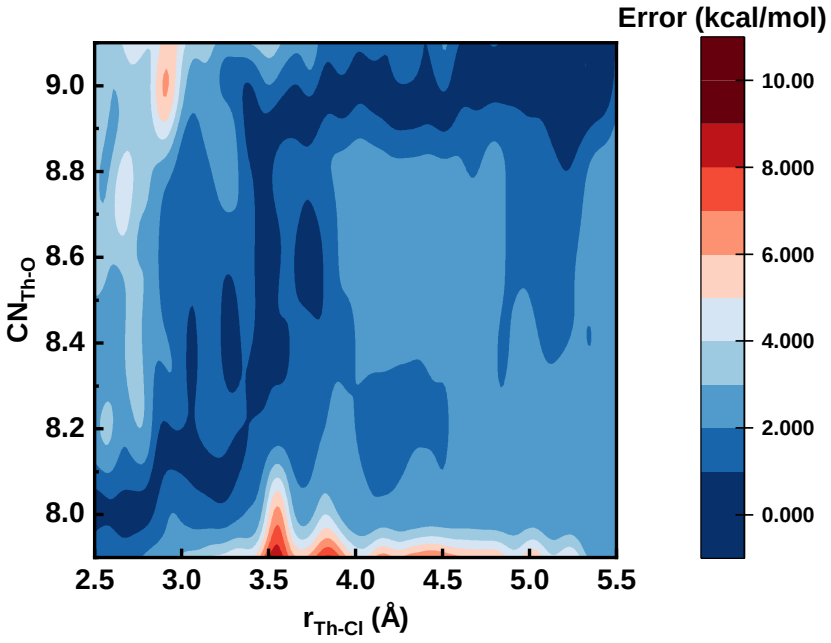

Fig. S6. Temporal convergence of 2D FES obtained from the metadynamics simulation.

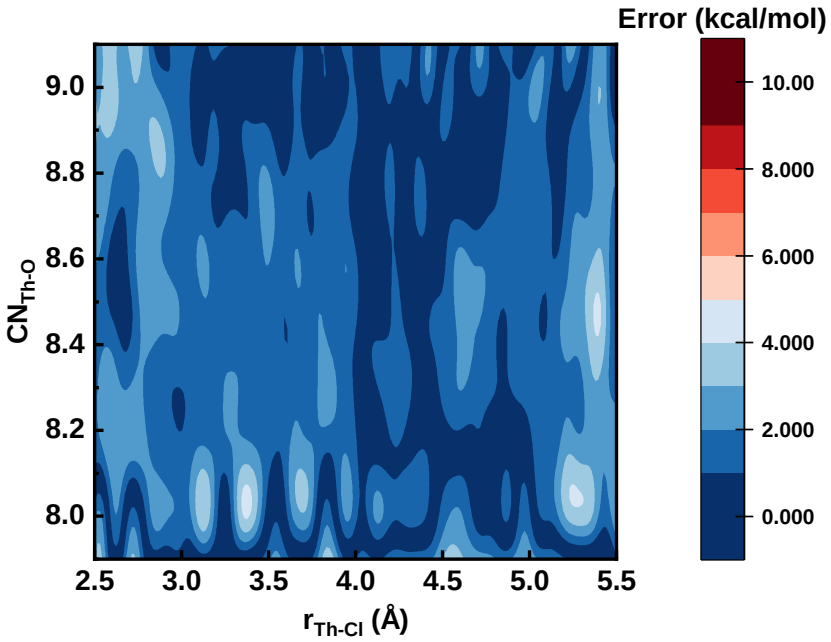

Fig. S7. Standard deviations between the results of a single converged metadynamics simulation and the statistical average results of three metadynamics simulations.

DFT calculations for energetics of 9-coordination and 10-coordination species.

Additional static DFT calculations were performed to determine the Gibbs free energy differences (ΔG) for the following two reactions:

$$Th(H_2O)_9^{4+} + H_2O \rightarrow Th(H_2O)_{10}^{4+} \quad (1)$$

$$Th(H_2O)_9(H_2O)_{17}^{4+} \rightarrow Th(H_2O)_{10}(H_2O)_{16}^{4+} \quad (2)$$

To account for the influence of the second solvation shell, the model in process 2 explicitly includes its water molecules. These calculations were executed using the AMS-2020.101 program.[4, 5] The scalar relativistic effects were incorporated using the zero-order regular approximation (ZORA) Hamiltonian.[6-8] The conductor-like screening model (COSMO)[9] was employed to describe the solvation effects of water. Grimme's D3 dispersion corrections with Becke-Johnson damping function were included in all calculations.[10, 11] All geometries were optimized in the PBE functional.[12] Vibrational frequencies were calculated to ensure that all structures were local minima and to obtain the thermal corrections. The low-frequency vibrational modes were modified by quasi-RRHO approximation.[13] To calculate the Gibbs free energy (G) of all species, the single-point energy calculations were executed in the PBE0[14], B3LYP[15] and TPSSh[16] functionals, which were well-tested for actinides[17].

In DFT calculations for energetics, the Gibbs free energy (G) was calculated by

$$G = E^{HL} + G_{corr}^{LL} + 1.89\ kcal/mol$$

where E^{HL} was the single-point energy calculated at the **high level** and G_{corr}^{LL} was the thermal correction calculated at the **low level**, the value of 1.89 kcal/mol was the correction from 1 bar standard state (gas phase, provided by most quantum chemistry codes) to 1 M standard state (solution).[18] The modified value of Gibbs free energy, G_m, was calculated by modifying the value of G_{corr}^{LL}. The approach can achieve the balance between accuracy and efficiency.[19, 20] The initial geometries used in the calculations were from the equilibrated trajectories from AIMD simulations. A more detailed description of the computational levels is given below.

Calculations at the **low level** (optimization and thermal correction):

Functional: PBE-D3(BJ)

Basis sets:

TZP for Th. The frozen core approximation was used for [$1s^2$-$4f^{14}$] of Th.

DZP for H and O.

Calculations at the **high level** (single-point energy):

Functional: B3LYP-D3(BJ) / PBE0-D3(BJ) / TPSSh-D3(BJ)

Basis sets: TZ2P for Th. TZP for H and O.

The relativistic ZORA basis sets,[21] which were built into the ADF-2020.101 program, were used in all calculations. The results are shown in Table S2. The positive values of ΔG indicate that the 9-coordination hydrated ion is thermodynamically more stable under the cluster model, confirming the results of AIMD simulations. However, MD simulations using metadynamics suggest that the stability difference between the 9-coordination state and the 10-coordination state is not obvious, and it is also proved by the uncertainties in the experimental results. Hence, the more positive values of ΔG_1 and $\Delta G_{1,m}$ indicate that the lack of an explicit description of the second solvation shell may lead to an overestimation of the stability of the 9-coordination species.

Table S2. Gibbs Free Energy Differences (kcal/mol) of Two Processes (ΔG_1 and ΔG_2) and the Modified Values with Quasi-RRHO Approximation ($\Delta G_{1,m}$ and $\Delta G_{2,m}$) Calculated in Different Functionals

	PBE0-D3(BJ)	B3LYP-D3(BJ)	TPSSh-D3(BJ)
ΔG_1	12.80	12.88	12.86
ΔG_2	6.93	6.19	6.97
$\Delta G_{1,m}$	13.15	13.23	13.21
$\Delta G_{2,m}$	9.31	8.57	9.35

Classical molecular dynamics (CMD) simulations for the hydration of Th^{4+}.

Both AIMD-based metadynamics calculations and static DFT calculations have demonstrated the stability of the 9-coordinated hydrated Th^{4+} ion. Considering that the interactions between Th^{4+} and water molecules are non-bonded in nature, it is also valuable to compare the results from CMD simulations over longer timescales with those obtained from AIMD simulations combined with enhanced sampling techniques. Therefore, we performed the CMD simulations using force field parameters fitted from experimental ion-oxygen distance (IOD) values for Th^{4+}, previously described in the literature.[22] We conducted following four sets of simulations with a timestep of 1 fs using the Gromacs 2018.8 software:[23]

	system	ensemble	size of water box	water model	time
A	Th^{4+} + 310 H_2O	NVT	$(21.01\ Å)^3$	TIP4P-Ew	40 ns
B	Th^{4+} + 310 H_2O	NVT	$(21.01\ Å)^3$	SPC/E	40 ns
	system	ensemble	ρ_{water}	water model	time
C	Th^{4+} + 3200 H_2O	NPT	1.024 g/cm^3	SPC/E	10 ns
D	Th^{4+} + 3200 H_2O	NPT	1.048 g/cm^3	TIP3P	10 ns

The results of these four CMD simulations were compared with our AIMD results (see Fig. S8). Specifically, these longer-timescale CMD simulations consistently report the values of $CN_{Th\text{-}O}$ ranging from 9 to 10, with three sets (A, C and D) converging closer to the $CN_{Th\text{-}O}$ of 9. It supports our results combined AIMD simulations with enhanced sampling, suggesting that the primary hydration number for Th^{4+} in aqueous solutions tends toward 9.

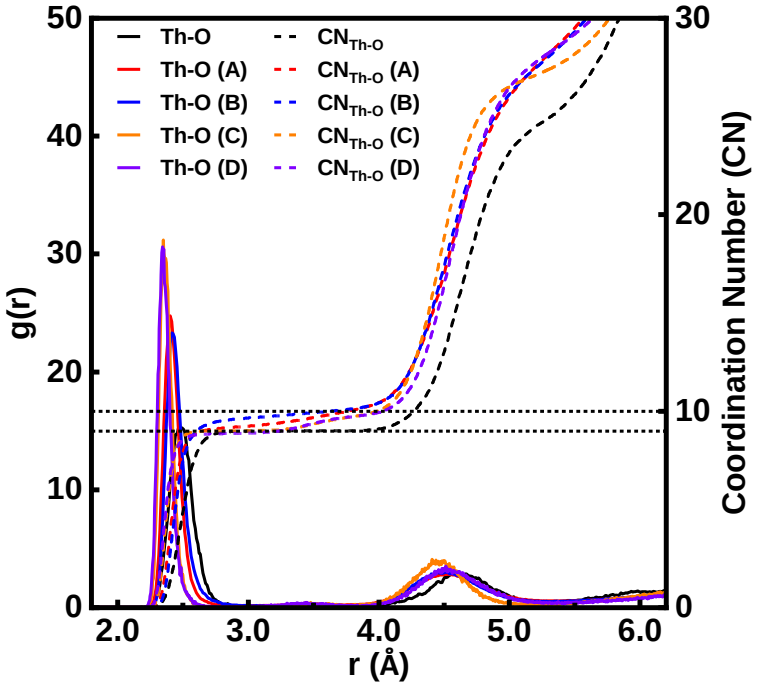

Fig. S8. Th-O RDFs and their integrated coordination numbers obtained from our AIMD simulation (in black) and the four different longer-timescale CMD simulations.

Partial charges of Th^{4+}.

To demonstrate the strong polarization caused by the highly charged Th^{4+} ion, we calculated three types of partial charges for Th^{4+} during the simulation process: Mulliken charges,[24-26] Hirshfeld charges,[27] and CM5 charges.[28] All calculations were performed using Multiwfn codes.[29] Specifically, we calculated the partial charges of Th^{4+} at every 2-ps interval across a 20-ps equilibrated trajectory from simulation no. 2. As shown in Fig. S9, Th^{4+} exhibits high positive charges in the 11 representative structures sampled from the equilibrated trajectory. Hirshfeld charges are lower compared to Mulliken and CM5 charges, a phenomenon that has been widely recognized in previous research.[30] The high partial charges of Th^{4+} are sufficient to lead to strong polarization effects on the surrounding aqueous environment. Furthermore, all three types of partial charges exhibit only slight fluctuations, suggesting that the chemical environment surrounding Th^{4+} remained relatively unchanged during the simulation. To some extent, this also implies the structural stability of the solvation shell surrounding Th^{4+}.

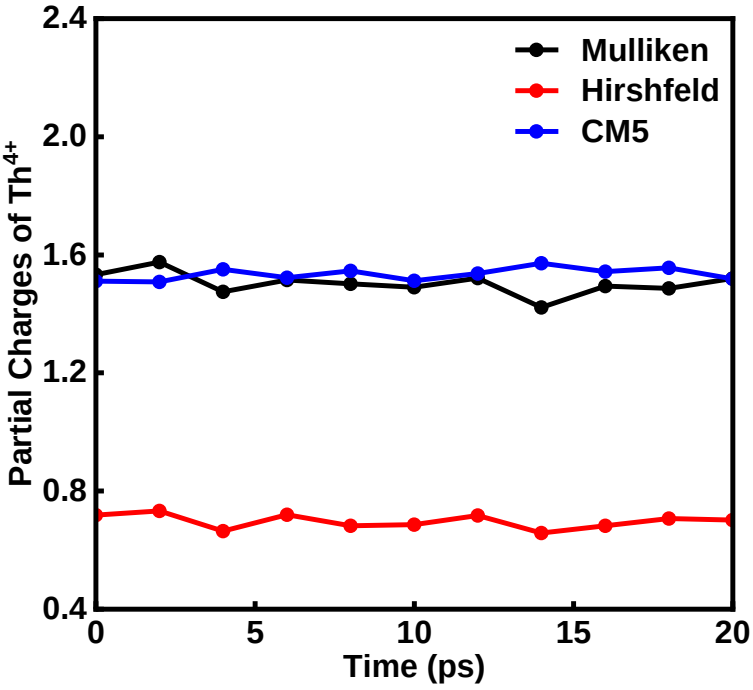

Fig. S9. Three types of calculated partial changes for Th^{4+} during the AIMD simulation.

MSD results for all water molecules in the solution and those in the two solvation shells of Th^{4+}.

To investigate the impact of temperature on dynamic properties, the MSDs of all water molecules in the solution and the water molecules in the two solvation shells of Th^{4+} at different temperatures were calculated. According to the Einstein relation,[31] the self-diffusion coefficient of the fluid has a clear linear relationship with the slope of the MSDs obtained from simulations using periodic boundary conditions at the long-time limit. The MSDs directly describe the diffusion process in the fluid. The MSD curves obtained from simulations at different temperatures are shown in the Fig. S10. An increase in temperature results in an increase in the slope of the MSD curves, both for overall water molecules and the water molecules in the solvation shells. In other words, an increase in temperature leads to an enhanced diffusivity of the water molecules. It is an expected conclusion that increased temperatures enhance the thermal motion of solvent molecules. It is noted that at the same temperature, the diffusivity of the water molecules in the solvation shells is always lower than that of all water molecules. The strong ion-solvent interactions ultimately result in a lower diffusion capacity of the water molecules in the solvation shells, which, to some extent, indicates the relatively structured solvation shells around Th^{4+}.

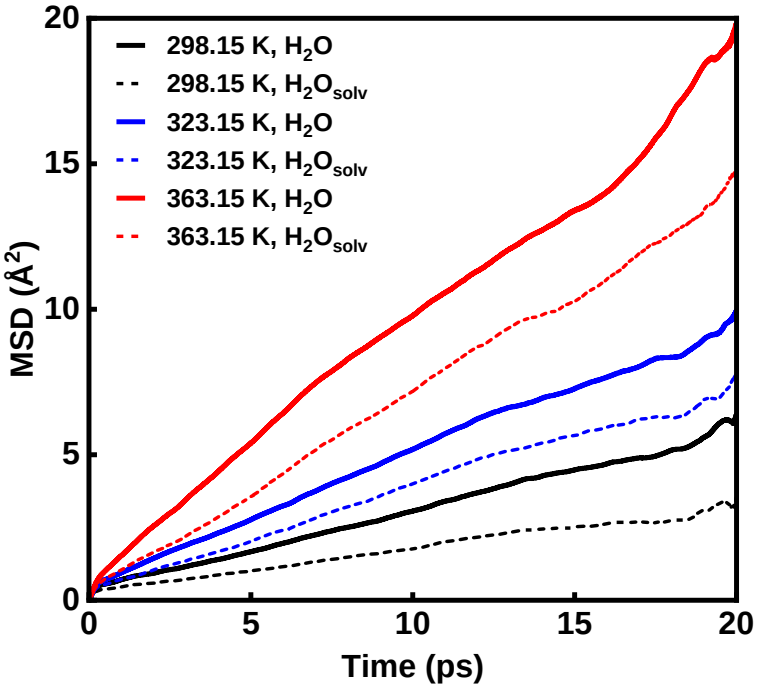

Fig. S10. MSDs of water molecules obtained from the simulations at different temperatures (298.15 K, 323.15 K and 363.15K). The MSDs of all water molecules (H_2O) are represented by solid lines, whereas the MSDs of the water molecules in the two solvation shells of Th^{4+} (H_2O_{solv}) are represented by dashed lines.

The O-O radial probability distribution (RPD) analysis.

In molecular dynamics simulations, the radial distribution function (RDF) is an important tool for analyzing the spatial distribution of particles. However, the value of the RDF, g(r), is commonly defined as the ratio of the average particle number density within a spherical shell between r and r + dr to the overall particle number density of the system, that is, $g(r) = \rho(r) / \rho$. This implies that with identical volumes, the values of g(r) cannot be directly compared between systems with different numbers of particles. To overcome this limitation, we introduce the radial probability distribution (RPD) as a new analytical approach to normalize RDF measurements, facilitating meaningful comparisons across systems irrespective of their particle number density.

In practical studies, the obtained g(r) consists of a series of discrete values. The RPD is defined for a specific radial distance r_0 as follows:

$$P(r_0) = \frac{g(r_0)}{\sum_i g(r_i)}$$

where $g(r_0)$ is the value of g(r) at r = r_0, and $\sum_i g(r_i)$ represents the sum of values of g(r) over discrete intervals ($r_i = r_{i-1} + dr$) within the analysis range from 0 to *r*. This normalization process effectively mitigates the influence of the system's average number density, allowing for a direct comparison of particle distribution features across systems with different particle number density.

In our work, the value of O-O RPD, $P_{OO}(r)$, was calculated for four different scenarios within simulation boxes of the same size:

1. Pure water (64 water molecules in the simulation box)
2. Th^{4+} aqueous solution (64 water molecules in the simulation box)
3. Water molecules in the first and second solvation shells of Th^{4+} (> 20 water molecules in the simulations box, $P_{OO,1\&2}(r)$)
4. Water molecules in the first solvation shell of Th^{4+} (9 water molecules in the simulations box, $P_{OO,1}(r)$)

We first calculated the O-O RDFs, $g_{OO}(r)$, for the aforementioned four scenarios with identical parameter settings, and then determined the values of $P_{OO}(r)$ for each case based on the given formula.

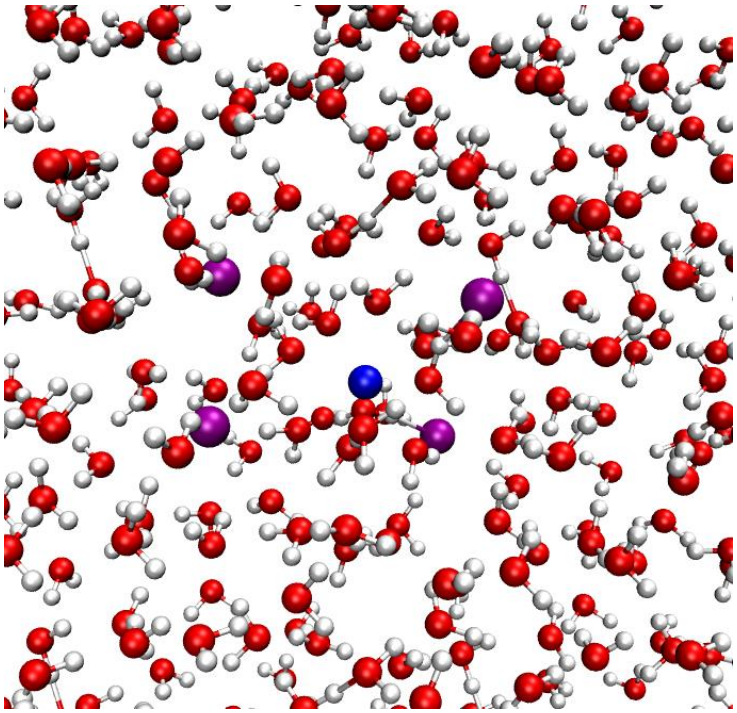

Fig. S11. A snapshot of the aqueous solution simulations including a Th^{4+} ion (blue), 64 water molecules with oxygen (red) and hydrogen (white) atoms, and 4 Cl^- anions (purple).

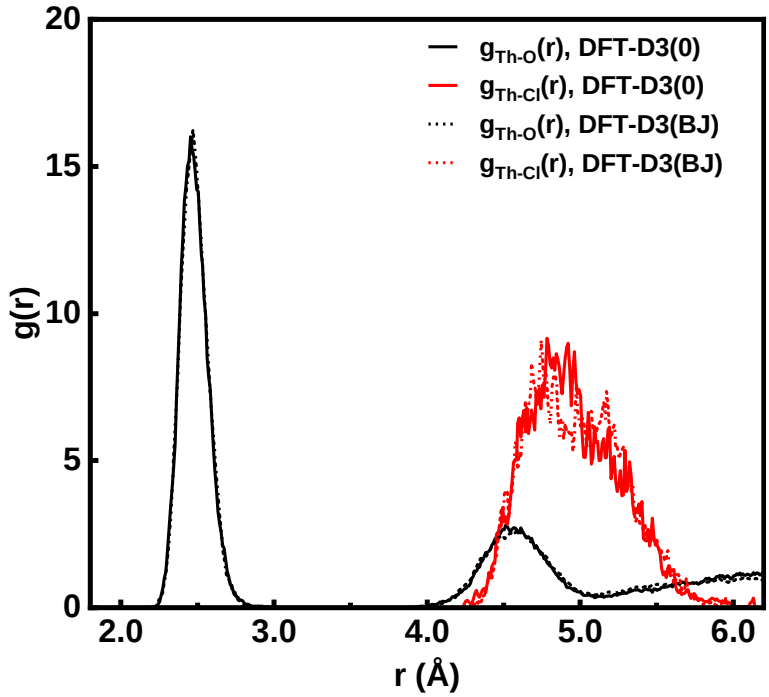

Fig. S12. Th-O RDFs and Th-Cl RDFs obtained from Th^{4+} - $4Cl^-$ - $64H_2O$ system at the PBE-D3(0) and PBE-D3(BJ) levels.

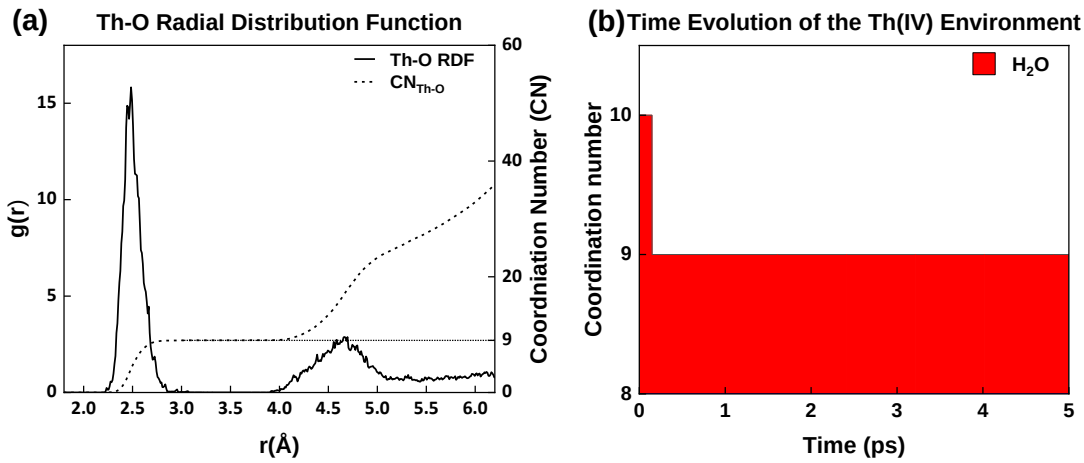

Fig. S13. (a) Th-O RDF obtained from the equilibrium phase simulation of the system including $Th(H_2O)_{10}^{4+}$. (b) Time evolution of the Th(IV) environment during the equilibrium phase simulation of the system including $Th(H_2O)_{10}^{4+}$. The total bar height is the total coordination number.

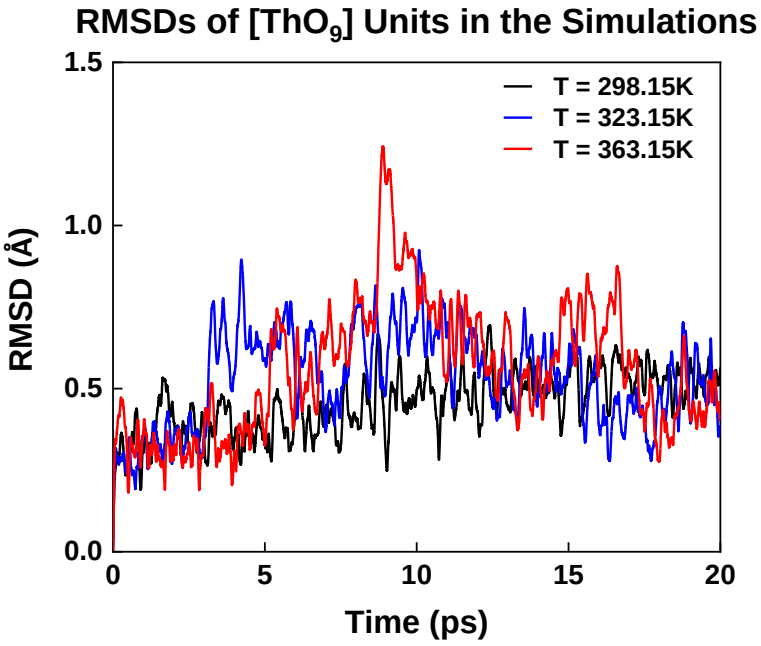

Fig. S14. The RMSDs of [ThO_9] structural units in the entire AIMD trajectories at different temperatures.

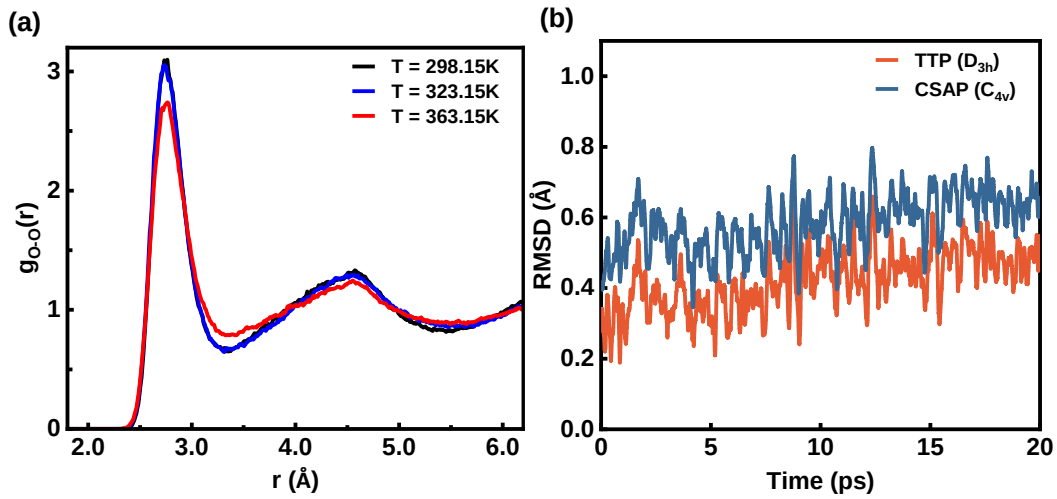

Fig. S15. (a) O-O RDFs at different temperatures. (b) The RMSDs between [ThO_9] structural units of each AIMD frame and the two reference geometries.

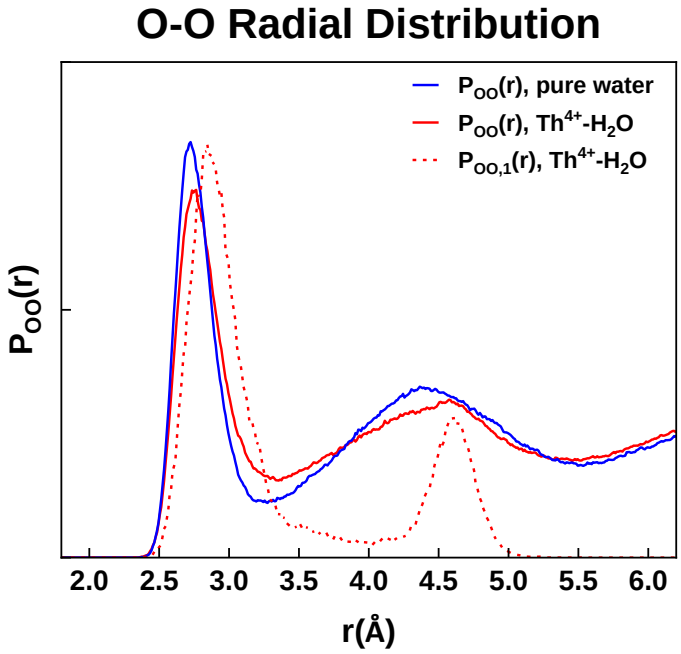

Fig. S16. O-O radial probability distribution ($P_{OO}(r)$) of water molecules in the FSS of Th^{4+}. $P_{OO,1}(r)$ is scaled by 0.5 times for clarity.

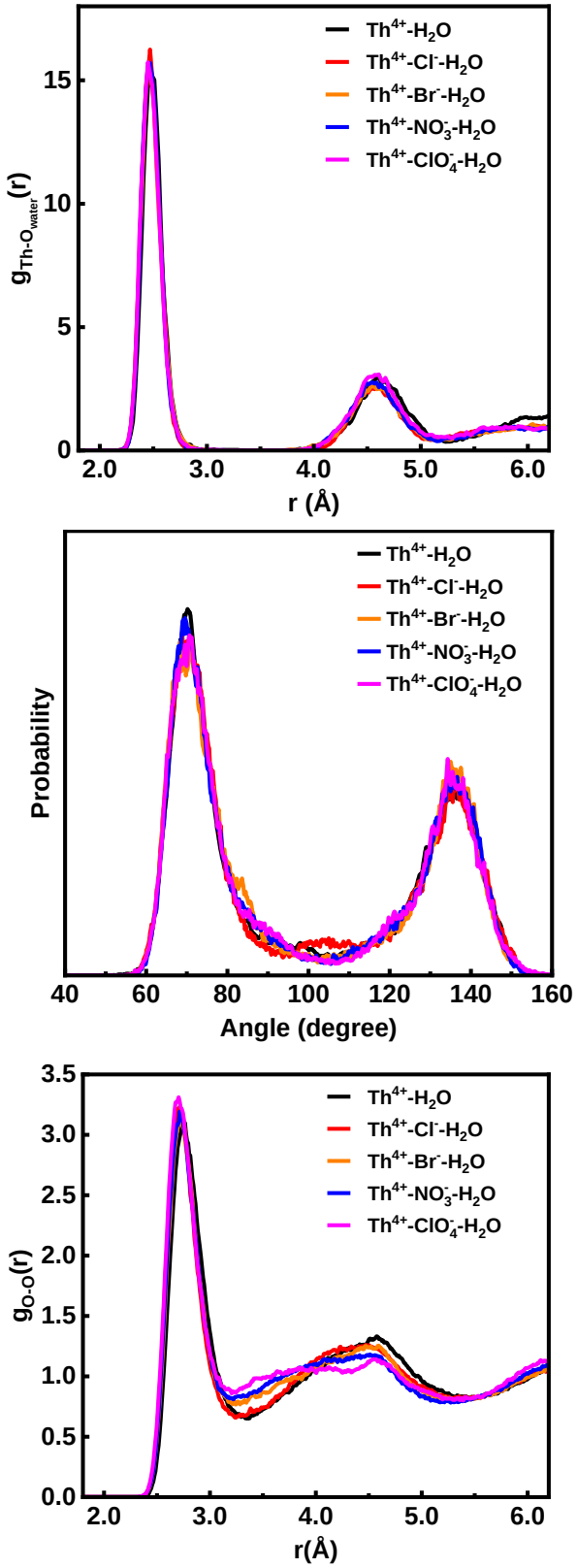

Fig. S17. Th-O_{water} RDFs (top), O-Th-O AnDFs (middle) and O-O RDFs (bottom) obtained from the simulations of the systems including Th^{4+} and counterions.

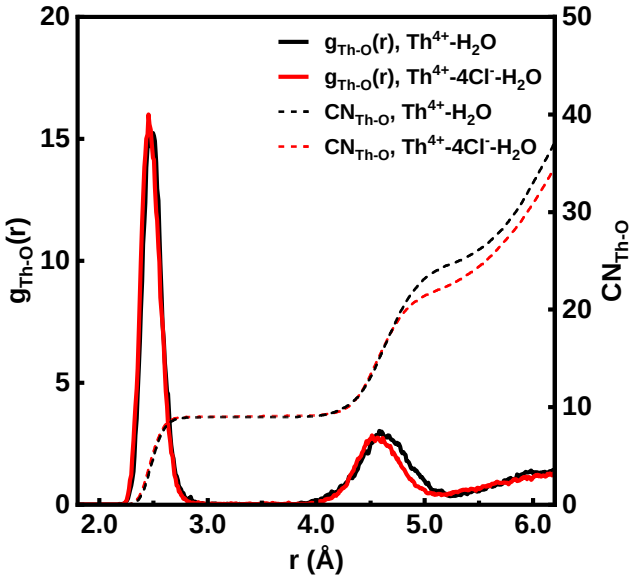

Fig. S18. Th-O RDFs and integrated coordination numbers obtained from simulations of the systems with and without Cl^- counterions.

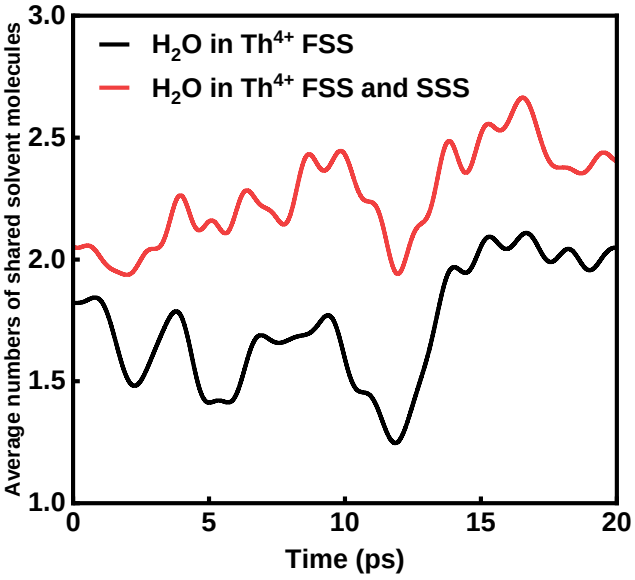

Fig. S19. Average numbers of solvent molecules shared between each Cl^- and Th^{4+} during the simulation.

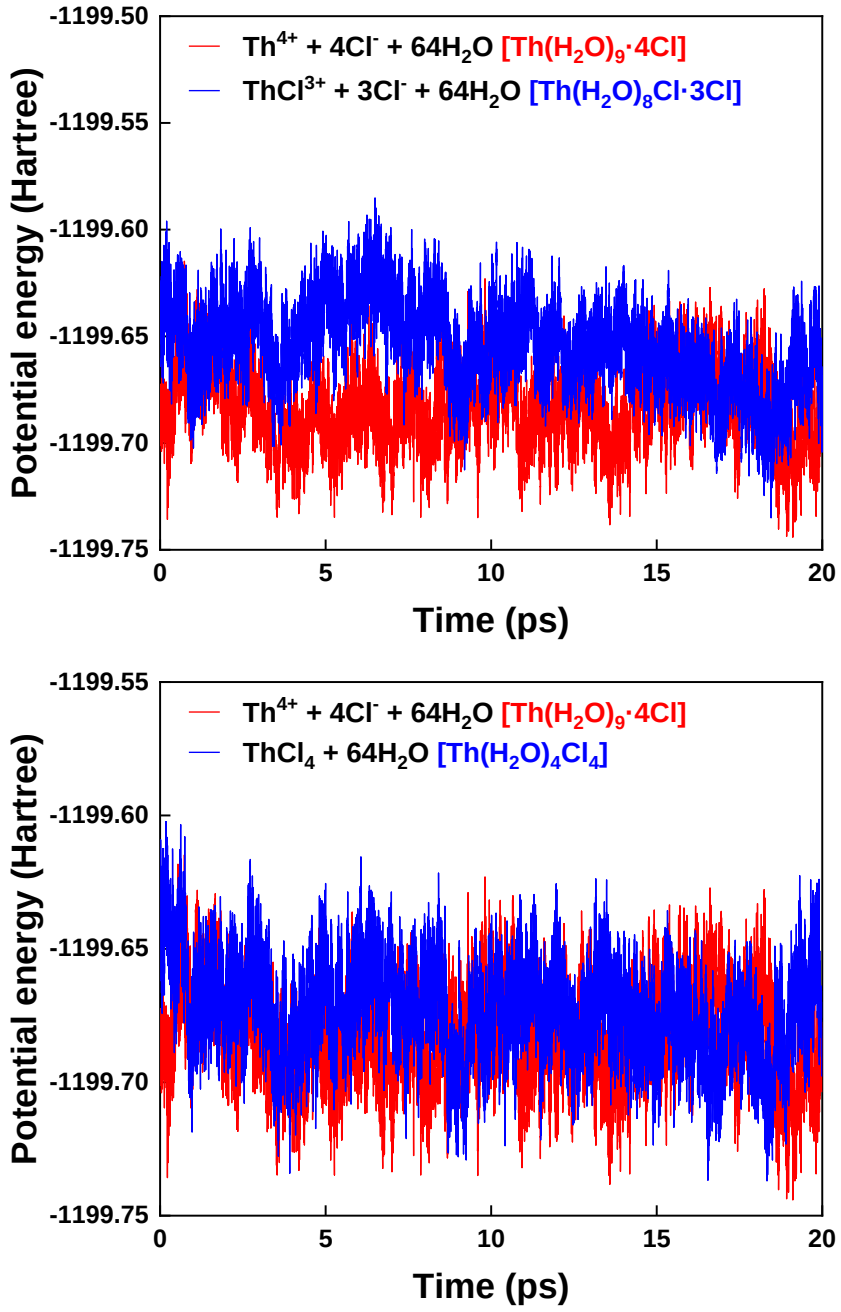

Fig. S20. The changes of potential energy of simulations including Th^{4+} - $4Cl^-$ SIPs and $ThCl^{3+}$ / $ThCl_4$ complex.

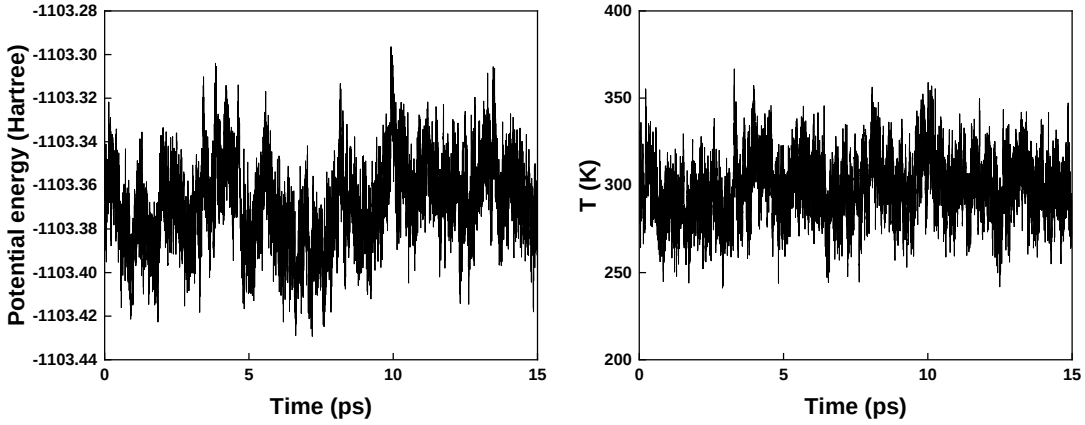

Fig. S21. The changes of potential energy and temperature of production phase simulation of simulation 1 (pure water).

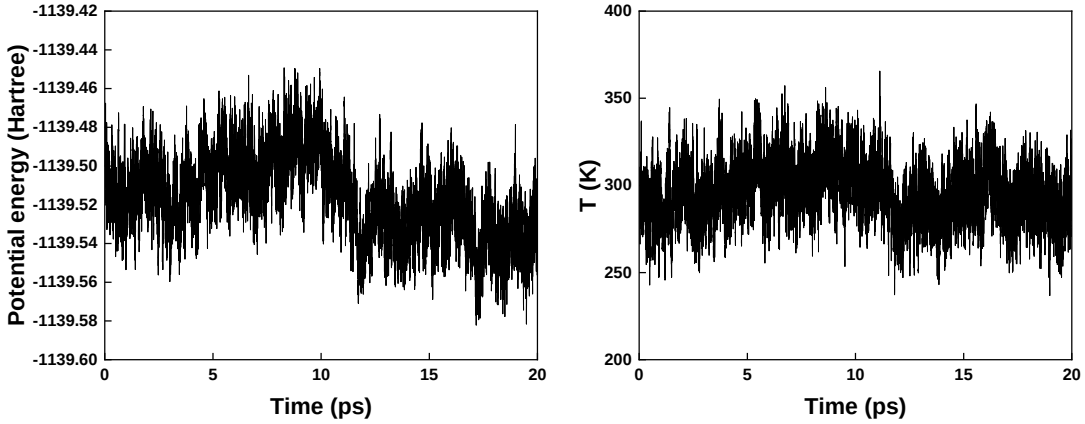

Fig. S22. The changes of potential energy and temperature of production phase simulation of simulation 2 ($Th(H_2O)_9^{4+}$ + $55H_2O$, 298.15K).

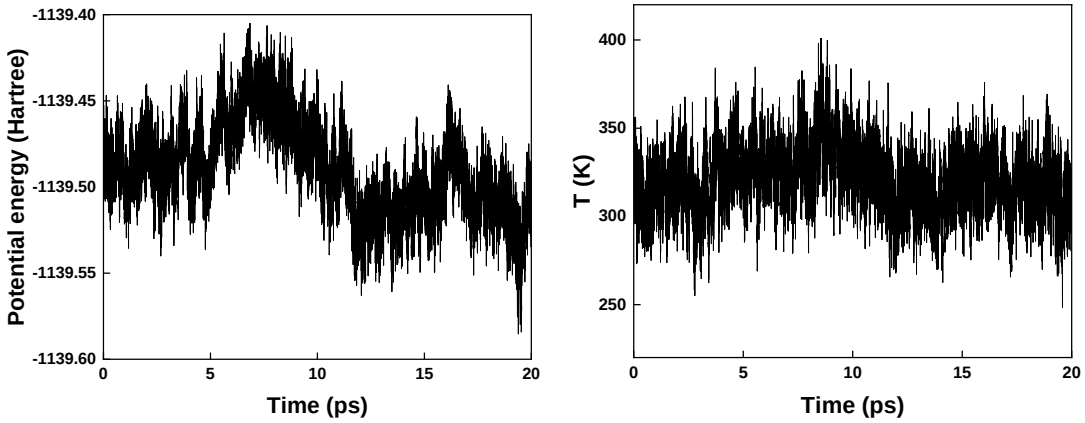

Fig. S23. The changes of potential energy and temperature of production phase simulation of simulation 3 ($Th(H_2O)_9^{4+}$ + $55H_2O$, 323.15K).

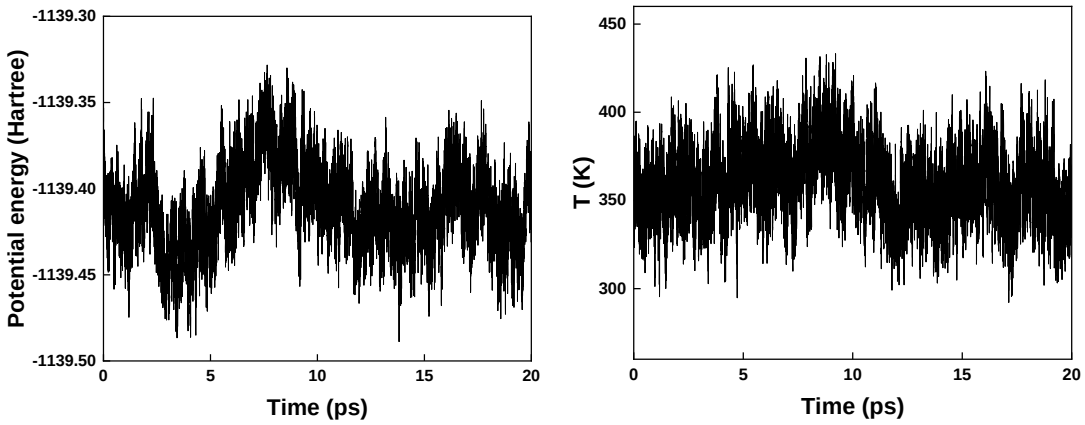

Fig. S24. The changes of potential energy and temperature of production phase simulation of simulation 4 ($Th(H_2O)_9^{4+}$ + $55H_2O$, 363.15K).

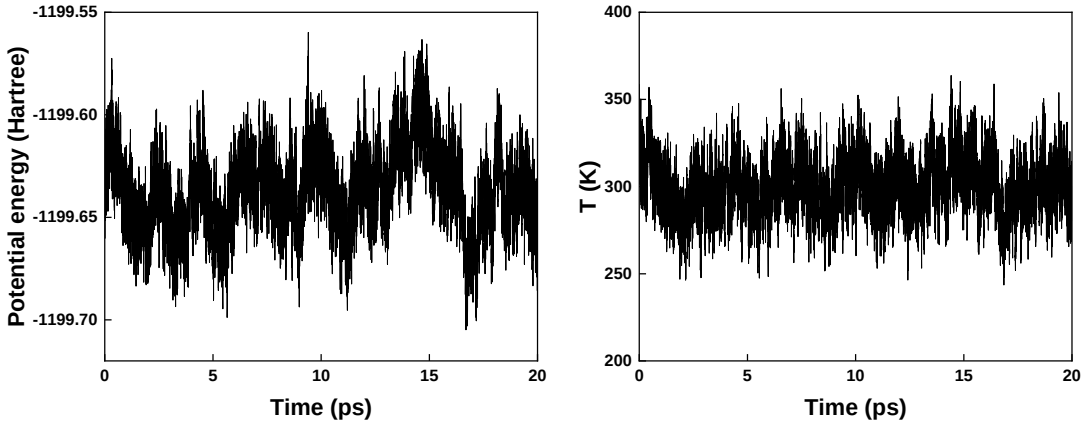

Fig. S25. The changes of potential energy and temperature of production phase simulation of simulation 5 ($Th(H_2O)_9^{4+}$ + $55H_2O$ + $4Cl^-$, 298.15K).

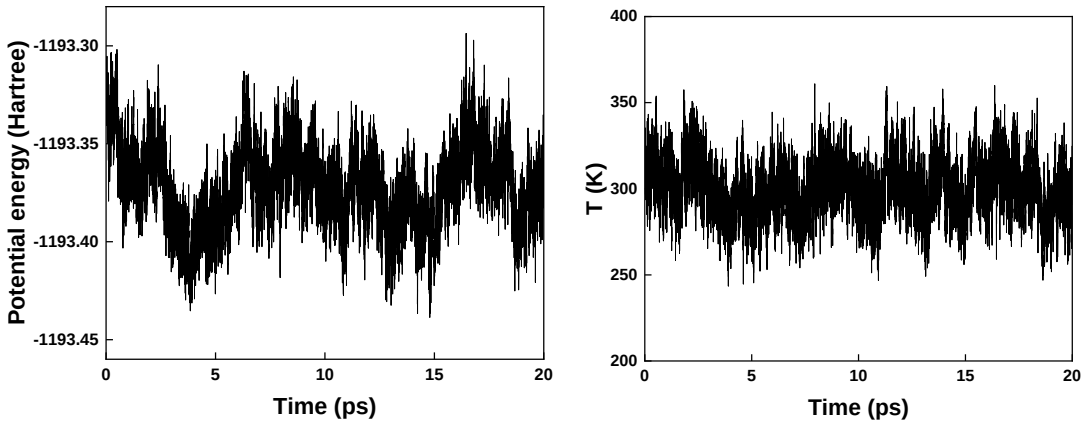

Fig. S26. The changes of potential energy and temperature of production phase simulation of simulation 6 ($Th(H_2O)_9^{4+}$ + $55H_2O$ + $4Br^-$, 298.15K).

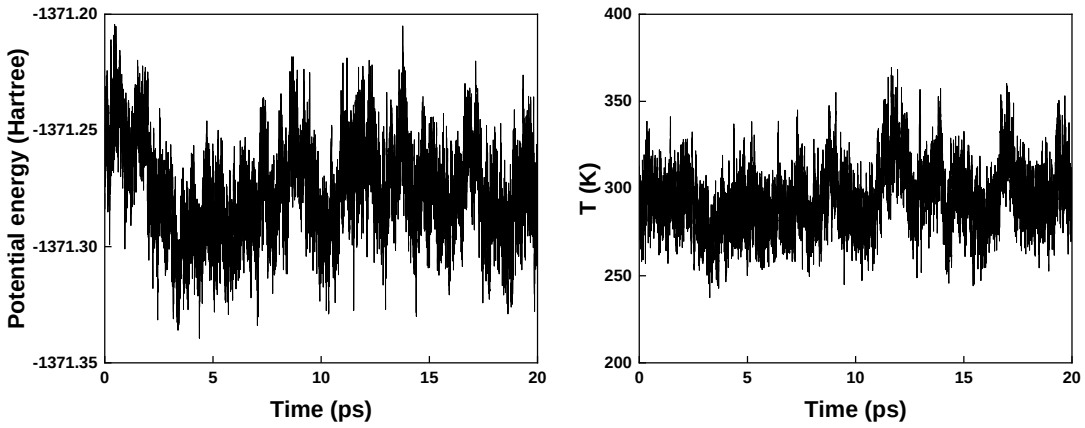

Fig. S27. The changes of potential energy and temperature of production phase simulation of simulation 7 ($Th(H_2O)_9^{4+}$ + $55H_2O$ + $4NO_3^-$, 298.15K).

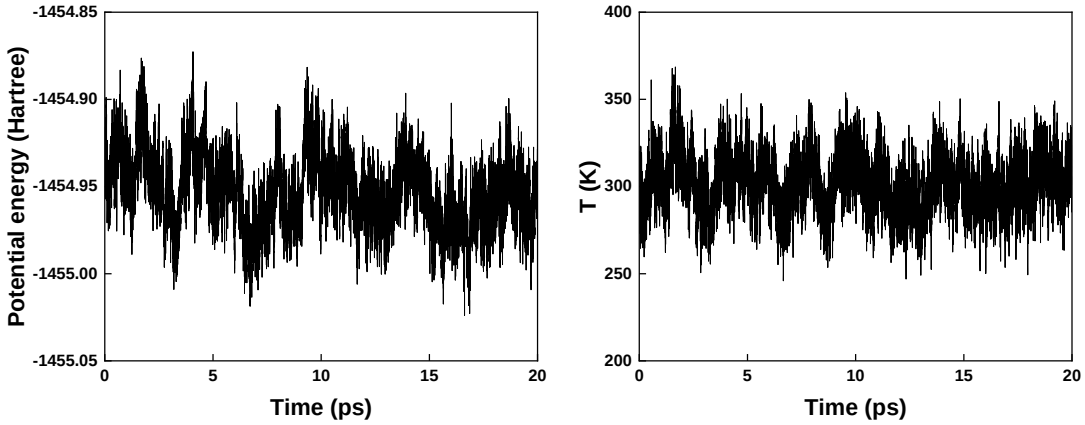

Fig. S28. The changes of potential energy and temperature of production phase simulation of simulation 8 ($Th(H_2O)_9^{4+}$ + $55H_2O$ + $4ClO_4^-$, 298.15K).

Tricapped Trigonal Prism Reference Geometry: (D_{3h} symmetry)

Th	6.21000000	6.21000000	6.21000000
O	6.21000000	8.71000001	6.21000000
O	7.33796758	7.17925066	4.20046217
O	4.66842436	6.45532764	4.25721766
O	7.08462666	4.46155747	4.65180332
O	4.65196501	4.27149870	5.95556011
O	6.54347450	4.46155746	7.96548952
O	4.12727219	6.45532763	7.57090385
O	6.64006741	7.17925066	8.47397774
O	8.62620230	6.71622985	6.60458567

Capped Square Antiprism Reference Geometry: (C_{4v} symmetry):

Th	6.21000000	6.21000000	6.21000000
O	6.21000000	8.26429786	4.78526834
O	6.21000000	6.21000000	3.71000000
O	4.15570214	6.21000000	4.78526834
O	6.21000000	4.15570214	4.78526834
O	4.75485974	4.75485974	7.62955404
O	7.66514026	4.75485974	7.62955404
O	4.75485974	7.66514026	7.62955404
O	7.66514026	7.66514026	7.62955404
O	8.26429786	6.21000000	4.78526834

References

1. R. Atta-Fynn, E. J. Bylaska and W. A. de Jong, *J. Phys. Chem. A.*, 2016, **120**, 10216-10222.

2. R. Atta-Fynn, E. J. Bylaska and W. A. de Jong, *J. Phys. Chem. Lett.*, 2013, **4**, 2166-2170.

3. A. Laio and F. L. Gervasio, *Rep. Prog. Phys.*, 2008, **71**, 126601.

4. G. te Velde, F. M. Bickelhaupt, E. J. Baerends, C. Fonseca Guerra, S. J. A. van Gisbergen, J. G. Snijders and T. Ziegler, *J. Comput. Chem.*, 2001, **22**, 931-967.

5. *ADF 2023.101*, SCM, Theoretical Chemistry, Vrije Universiteit, Amsterdam, The Netherlands. http://www.scm.com.

6. E. van Lenthe, A. Ehlers and E.-J. Baerends, *J. Chem. Phys.*, 1999, **110**, 8943-8953.

7. E. van Lenthe, R. van Leeuwen, E. J. Baerends and J. G. Snijders, *Int. J. Quantum Chem.*, 1996, **57**, 281-293.

8. E. van Lenthe, E. J. Baerends and J. G. Snijders, *J. Chem. Phys.*, 1994, **101**, 9783-9792.

9. C. C. Pye and T. Ziegler, *Theor. Chem. Acc.*, 1999, **101**, 396-408.

10. S. Grimme, S. Ehrlich and L. Goerigk, *J. Comput. Chem.*, 2011, **32**, 1456-1465.

11. S. Grimme, J. Antony, S. Ehrlich and H. Krieg, *J. Chem. Phys.*, 2010, **132**, 154104.

12. J. P. Perdew, K. Burke and M. Ernzerhof, *Phys. Rev. Lett.*, 1996, **77**, 3865-3868.

13. S. Grimme, *Chem. Eur. J.*, 2012, **18**, 9955-9964.

14. C. Adamo and V. Barone, *J. Chem. Phys.*, 1999, **110**, 6158-6170.

15. P. J. Stephens, F. J. Devlin, C. F. Chabalowski and M. J. Frisch, *J. Phys. Chem.*, 1994, **98**, 11623-11627.

16. V. N. Staroverov, G. E. Scuseria, J. Tao and J. P. Perdew, *J. Chem. Phys.*, 2003, **119**, 12129-12137.

17. L. E. Aebersold and A. K. Wilson, *J. Phys. Chem. A.*, 2021, **125**, 7029-7037.

18. J. H. Jensen, *Phys. Chem. Chem. Phys.*, 2015, **17**, 12441-12451.

19. M. Wang, X. He, M. Taylor, W. Lorpaiboon, H. Mun and J. Ho, *J. Chem. Theory*

Comput., 2023, **19**, 5036-5046.

20. B. Chan and J. Ho, *J. Phys. Chem. A.*, 2023, **127**, 10026-10031.

21. E. Van Lenthe and E. J. Baerends, *J. Comput. Chem.*, 2003, **24**, 1142-1156.

22. P. Li, L. F. Song and K. M. Merz, Jr., *J. Phys. Chem. B.*, 2015, **119**, 883-895.

23. M. J. Abraham, T. Murtola, R. Schulz, S. Páll, J. C. Smith, B. Hess and E. Lindahl, *SoftwareX*, 2015, **1-2**, 19-25.

24. R. S. Mulliken, *J. Chem. Phys.*, 1955, **23**, 1841-1846.

25. R. S. Mulliken, *J. Chem. Phys.*, 1955, **23**, 1833-1840.

26. R. S. Mulliken, *J. Chem. Phys.*, 1955, **23**, 2338-2342.

27. F. L. Hirshfeld, *Theor. Chim. Acta*, 1977, **44**, 129-138.

28. A. V. Marenich, S. V. Jerome, C. J. Cramer and D. G. Truhlar, *J. Chem. Theory Comput.*, 2012, **8**, 527-541.

29. T. Lu and F. Chen, *J. Comput. Chem.*, 2012, **33**, 580-592.

30. T. Lu and Q. Chen, in *Exploring Chemical Concepts Through Theory and Computation*, ed. S. Liu, Wiley - VCH, 2024, DOI: 10.1002/9783527843435.ch6, pp. 161-188.

31. M. P. Allen and D. J. Tildesley, *Computer Simulation of Liquids*, Oxford University Press, 2nd edn., 2017.